Inorganic Chemistry
Article

Inorg. Chem. **2009**, *48*, 6251–6260 **6251**
DOI: 10.1021/ic900552b

Multielectron Redox Activity Facilitated by Metal−Metal Interactions in Early/Late Heterobimetallics: Co/Zr Complexes Supported by Phosphinoamide Ligands

Bennett P. Greenwood, Scott I. Forman, Gerard T. Rowe, Chun-Hsing Chen, Bruce M. Foxman, and Christine M. Thomas*

Department of Chemistry, Brandeis University, 415 South Street, Waltham, Massachusetts 02454

Received March 23, 2009

To assess the effect of dative M→M interactions on redox properties in early/late heterobimetallic complexes, a series of Co/Zr complexes supported by phosphinoamide ligands have been synthesized and characterized. Treatment of the Zr metalloligands $(Ph_2PN^iPr)_3ZrCl$ (**1**), $(^iPr_2PNMes)_3ZrCl$ (**2**), and $(^iPr_2PN^iPr)_3ZrCl$ (**3**) with CoI_2 leads to reduction from Co^{II} to Co^{I} and isolation of the heterobimetallic complexes $ICo(Ph_2PN^iPr)_3ZrCl$ (**4**), $ICo(^iPr_2PNMes)_3ZrCl$ (**5**), and $ICo(^iPr_2PN^iPr)_3ZrCl$ (**6**), respectively. Interestingly, treatment of CoI_2 with the phosphinoamine Ph_2PNH^iPr in the absence of a bound Zr center leads to the disubstituted Co^{II} complex $(Ph_2PNH^iPr)_2CoI_2$ (**7**). The tris(phosphinoamine) Co^{I} complex $(Ph_2PNH^iPr)_3CoI$ (**8**) can only be generated in the presence of an added reductant such as Zn^0, indicating that the reduction of Co^{II} to Co^{I} only occurs in the presence of Zr in the formation of complexes **4**−**6**. Structural characterization of **4**−**6** reveals a Zr−Co interaction, with interatomic distances of 2.7315(5) Å, 2.6280(5) Å, and 2.6309(5) Å, respectively. This distance appears to decrease as the phosphine donors on Co become more electron-releasing, strengthening the dative Co→Zr interaction. Cyclic voltammetry of **4**−**6** shows that all three compounds can be further reduced by two electrons at relatively mild reduction potentials (−1.65 V to −2.07 V vs Fc/Fc^+). The potentials at which these reductions occur in each of these complexes are largely governed by the extent to which electron-density is donated to Zr, as well as the electron-donating ability of the phosphine substituents. Moreover, cyclic voltammetry of complex **8** reveals that in the absence of Zr, the Co center is significantly more electron rich, and thus more difficult to reduce. Chemical reduction of **5** leads to the isolation of the two-electron reduced dinitrogen complex $[N_2Co(^iPr_2PNMes)_3ZrX][Na(THF)_5]$ (**9**). X-ray crystallography of **9** reveals that two-electron reduction is accompanied by a significant contraction of the Co−Zr interatomic distance from 2.6280(5) Å to 2.4112(3) Å. These heterobimetallic complexes have been studied computationally using density functional theory to examine the nature of the metal−metal interactions in these species.

Introduction

In recent years, dinuclear complexes containing two different transition metal centers have received increasing interest owing to the presumption that their reactivity should vary substantially from that of monometallic complexes or homobimetallic complexes.[1] In particular, early/late heterobimetallic complexes featuring interactions between a hard, Lewis acidic early metal center and a soft, Lewis basic late metal center are particularly interesting targets in light of their two vastly different reaction sites which lead to potential applications as bifunctional catalysts for the activation of small molecule substrates and homogeneous catalysis. While a number of early/late heterobimetallic complexes have been synthesized, the nature of the metal−metal interactions in these complexes and the effect of these interactions on redox behavior and reactivity remains largely unexplored. Moreover, the metal−metal interactions in early/late heterobimetallics are analogous to metal→borane interactions that have received recent attention in metalloboratrane complexes.[2] These types of Z-type bonding interactions, in which a metal center datively donates an electron-pair to a ligand atom, are intriguing in that the *effective* oxidation state of the metal center is higher than that predicted as the *formal* oxidation state, as result of electron withdrawal by the Z-type ligand.[3]

Early/late heterobimetallic complexes linked by alkoxyalkylphosphines $[Ph_2PCH_2O]^-$ were synthesized by Wolczanski and

*To whom correspondence should be addressed. E-mail: thomasc@brandeis.edu.

(1) (a) Stephan, D. W. *Coord. Chem. Rev.* **1989**, *95*, 41. (b) Wheatley, N.; Kalck, P. *Chem. Rev.* **1999**, *99*, 3379.

(2) (a) Figueroa, J. S.; Melnick, J. G.; Parkin, G. *Inorg. Chem.* **2006**, *45*, 7056. (b) Hill, A. F.; Owen, G. R.; White, A. J. P.; Williams, D. J. *Angew. Chem., Int. Ed.* **1999**, *38*, 2759. (c) Sircoglou, M.; Bontemps, S.; Bouhadir, G.; Saffon, N.; Miqueu, K.; Gu, W.; Mercy, M.; Chen, C.-H.; Foxman, B. M.; Maron, L.; Ozerov, O. V.; Bourissou, D. *J. Am. Chem. Soc.* **2008**, *130*, 16729. (d) Bontemps, S.; Sircoglou, M.; Bouhadir, G.; Puschmann, H.; Howard, J. A. K.; Dyer, P. W.; Miqueu, K.; Bourissou, D. *Chem.—Eur. J.* **2008**, *14*, 731–740. (e) Sircoglou, M.; Bontemps, S.; Mercy, M.; Saffon, N.; Takahashi, M.; Bouhadir, G.; Maron, L.; Bourissou, D. *Angew. Chem., Int. Ed.* **2007**, *46*, 8583.

(3) (a) Green, M. L. H. *J. Organomet. Chem.* **1995**, *500*, 127–148. (b) Parkin, G. *Organometallics* **2006**, *25*, 4744.

Published on Web 06/05/2009

co-workers several decades ago in an effort to model the interactions between electron-rich late metals and early metal oxide surfaces.[4] More recently, Nagashima et al. have utilized titanium and zirconium complexes supported by phosphinoamides, $[Ph_2PNR]^-$ (where R = ^{i}Pr or ^{t}Bu), as metalloligands for late transition metal centers.[5] The disubstituted titanium complex $(Ph_2PN^tBu)_2TiCl_2$ was utilized as a bidentate ligand in Ni^{II}, Pd^{II}, and Pt^{II} allyl complexes, and it was found that the M→Ti interactions in these complexes reduced the electron density at the late transition metal and, in turn, greatly enhanced the electrophilicity of the M-bound allyl moiety.[5d] In addition, the trisubstituted zirconium complexes $(Ph_2PNR)_2ZrCl$ were coordinated to $Mo^0(CO)_3$ and Cu^ICl fragments in a tridentate, tripodal fashion. Nagashima and co-workers found that in the $(CO)_3Mo(Ph_2PN^iPr)_3ZrCl$ complex, the CO stretching frequencies are shifted 50−70 cm^{-1} higher than comparable $(CO)_3Mo$(triphos) complexes as a result of weaker back-bonding into CO π^* orbitals.[5c] In light of this, we were curious to ascertain what effect coordination of a Lewis acidic early transition metal would have on a potentially redox-active late transition metal. Such a dative M_1→M_2 interaction would be expected to reduce the electron density at M_1, and therefore could facilitate reduction and small molecule activation at milder potentials. In a related study, Berry and co-workers have examined heterobimetallic interactions in Cr≡Cr−Fe complexes, and found that the metal−metal multiply bonded moieties donate electron density to the Fe center, resulting in a *trans* influence and significantly lowering the $Fe^{III/II}$ potential in these complexes.[6]

Results and Discussion

Synthesis of Co/Zr Heterobimetallic Complexes 4−6. For this investigation, we chose to explore heterobimetallics with a series of phosphinoamide ligands of differing electronic properties. The phosphinoamine precursors Ph_2PNH^iPr, $^iPr_2PNHMes$ (Mes = 2,4,6-trimethylphenyl), and $^iPr_2PNH^iPr$ were prepared using modifications of literature procedures.[7] In a procedure similar to that previously described, deprotonation of the phosphinoamines with 1 equiv of ^{n}BuLi at −78 °C, followed by treatment with 1/3 equiv of $ZrCl_4$, led to isolation of the zirconium metalloligands $(Ph_2PN^iPr)_3ZrCl$ (**1**), $(^iPr_2PNMes)_3ZrCl$ (**2**), and $(^iPr_2PN^iPr)_3ZrCl$ (**3**) in moderate to good yield.[5c] Previously, Nagashima and co-workers showed through X-ray crystallography and variable temperature ^{1}H NMR that the phosphines in **1** are unequivocally bound to the Zr center at low temperature and in the solid state, while reversible phosphine dissociation occurs in solution at room temperature.[5c] Although only one ^{31}P NMR signal is observed at all temperatures, variable temperature ^{1}H NMR spectra of **2** and **3** confirm that these complexes exhibit the same dynamic behavior, making these derivatives viable metalloligands as well.[8] Accordingly, treatment of **1**, **2**, and **3** with 1 equiv of CoI_2 led to isolation of heterobimetallic Zr/Co complexes as shown in Scheme 1. Surprisingly, the cobalt centers in the green paramagnetic products $ICo(Ph_2PN^iPr)_3ZrCl$ (**4**), $ICo(^iPr_2PNMes)_3ZrCl$ (**5**), and $ICo(^iPr_2PN^iPr)_3ZrCl$ (**6**), respectively, had been formally reduced from Co^{II} to Co^I. The oxidation states of **4**, **5**, and **6** were confirmed by their solution magnetic moments corresponding to $S = 1$ (μ_{eff} = 2.92, 2.87, and 3.10 μ_B, respectively). Evidence for Co→Zr interactions in **4**−**6** provided by structural characterization using X-ray crystallography, computational studies using density functional theory (DFT), and dramatic effects on redox activity will be discussed later in this manuscript.

Scheme 1

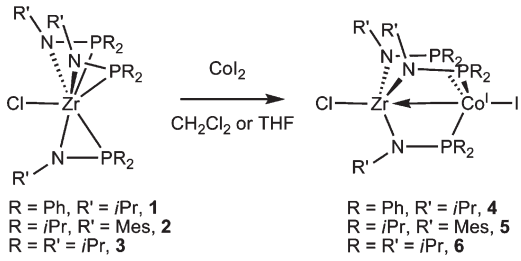

In attempts to synthesize derivatives featuring other metal combinations, we found that reactions of **1**−**3** with metal salts with a less accessible $M^{II/I}$ redox potential such as $FeCl_2$, FeI_2, and $ZnCl_2$ did not lead to heterobimetallic complexes. In addition, $CoCl_2$ also was an ineffective starting material for the preparation of mixed metal derivatives. In light of this halide dependence, it is likely that the reducing agent is I^-, and the resulting I_2 is subsequently consumed via reaction with the phosphines in **1**−**3**.[9−11] Nonetheless, it is evident that the close proximity of the Lewis acidic Zr center enforced by the phosphinoamide ligand geometry necessitates reduction of the late transition metal center to a more Lewis basic +1 oxidation state upon or prior to coordination. To provide further evidence that the reduction to Co^I in

(4) (a) Ferguson, G. S.; Wolczanski, P. T. *Organometallics* **1985**, *4*, 1601. (b) Ferguson, G. S.; Wolczanski, P. T. *J. Am. Chem. Soc.* **1986**, 108. (c) Ferguson, G. S.; Wolczanski, P. T.; Párkányi, M. C.; Zonnevylle, M. C. *Organometallics* **1988**, *7*, 1967. (d) Baxter, S. M.; Ferguson, G. S.; Wolczanski, P. T. *J. Am. Chem. Soc.* **1988**, *110*, 4231.

(5) (a) Nagashima, H.; Sue, T.; Oda, T.; Kanemitsu, A.; Matsumoto, T.; Motoyama, Y.; Sunada, Y. *Organometallics* **2006**, *25*, 1987. (b) Sunada, Y.; Sue, T.; Matsumoto, T.; Nagashima, H. *J. Organomet. Chem.* **2006**, *691*, 3176. (c) Sue, T.; Sunada, Y.; Nagashima, H. *Eur. J. Inorg. Chem.* **2007**, 2897. (d) Tsutsumi, H.; Sunada, Y.; Shiota, Y.; Yoshizawa, K.; Nagashima, H. *Organometallics* **2009**, *28*, 1988.

(6) (a) Nippe, M.; Berry, J. F. *J. Am. Chem. Soc.* **2007**, *129*, 12684. (b) Nippe, M.; Victor, E.; Berry, J. F. *Eur. J. Inorg. Chem.* **2008**, 5569.

(7) (a) Sisler, H. H.; Smith, N. L. *J. Org. Chem.* **1961**, *26*, 611. (b) Poetschke, N.; Nieger, M.; Khan, M. A.; Niecke, E.; Ashby, M. T. *Inorg. Chem.* **1997**, *36*, 4087.

(8) Additional experimental details are included in the Supporting Information for this manuscript.

(9) The potential for the $2I^- \rightarrow I_2 + 2e^-$ couple is −0.14 V vs ferrocene (in MeCN) as reported in: Connelly, N. G.; Geiger, W. E. *Chem. Rev.* **1996**, *96*, 877–910.

(10) I_2 reacts stoichiometrically with $LiN(PPh_2)_2$ to effect P-P coupling: Braunstein, P.; Hasselbring, R.; Tiripicchio, A.; Ugozzoli, F. *J. Chem. Soc., Chem. Commun.* **1995**, 37–38. We have also confirmed that I_2 is consumed quantitatively by both our phosphinoamines and our zirconium phosphinoamide complexes. Stoichiometric reaction of Ph_2PNH^iPr with I_2 in C_6D_6 leads to complete consumption of both I_2 (based on disappearance of the diagnostic purple color) and Ph_2PNH^iPr (based on disappearance of its ^{31}P NMR signal) to form a highly insoluble red/orange material. Likewise, stoichiometric reaction of **2** with I_2 leads to complete consumption of both materials and appearance of new phosphorus-containing products.

(11) Preliminary data suggests that the reaction of **2** with $CoCl_2$ indeed leads to a heterobimetallic product in the presence of an external reductant such as $NaBH_4$, based on the similarity of ^{1}H NMR features to those of **5** in the crude NMR of this reaction.

Scheme 2

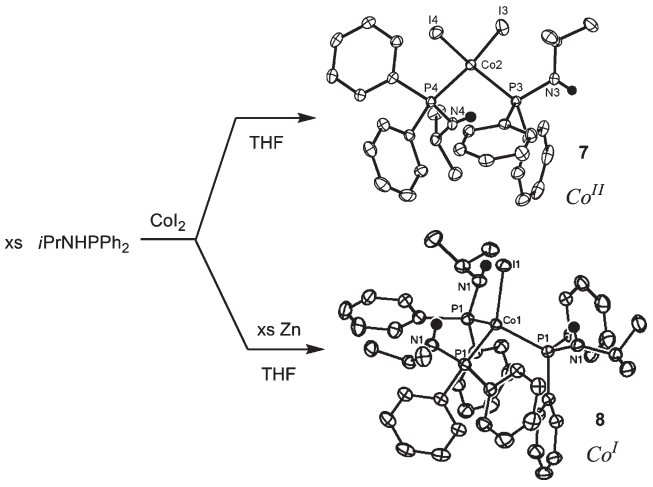

complexes **4**−**6** is unequivocally a result of the Zr's presence, the reaction of CoI_2 with the phosphinoamine Ph_2PNH^iPr was examined in the absence of a tethered Zr center (Scheme 2). Indeed, treatment of CoI_2 with excess Ph_2PNH^iPr led exclusively to the red disubstituted Co^{II} product $(Ph_2PNH^iPr)_2CoI_2$ (**7**), as confirmed structurally and spectroscopically.[8] The Co^{I} trisubstituted complex $(Ph_2PNH^iPr)_3CoI$ (**8**) could be synthesized, but only in the presence of elemental Zn as a reducing agent. Much like **4**−**6**, complex **8** is green and paramagnetic, with a solution magnetic moment indicative of high spin Co^{I} ($\mu_{eff} = 2.89\ \mu_B$).

Structural Characterization of Co/Zr Heterobimetallic Complexes 4−6. Single crystals of complexes **4**, **5**, and **6** were grown and subjected to X-ray diffraction. The molecular structures of **4**−**6** are shown in Figure 1 and relevant interatomic distances and angles are tabulated in Table 1. All three complexes have C_{3v} symmetry with an essentially tetrahedral geometry at the Co center. The P−Co−P angles in all three complexes are within 5° of the expected 109.5° angle between ligands in an ideal tetrahedron. Furthermore, the average P−Co−P angles in **4**−**6** are only slightly expanded (∼2−4°) from the P−Co−P angles in monometallic complex **8**. Thus, there is no significant structural distortion from tetrahedral geometry to trigonal bipyramidal geometry at Co in complexes **4**−**6** as a result of interactions between Co and Zr. However, the geometry about Zr clearly indicates a structural distortion toward trigonal bipyramidal geometry in all three complexes. The average N−Zr−N angles in **4**−**6** are very close to 120° (118.6°, 119.5°, and 119.5°, respectively) and the sum of the three N−Zr−N angles is 356−359°, as would be expected for the angles in an ideal trigonal bypyramid. In addition, the average N−Zr−Co angles in **4**−**6** are close to 90° (83.2°, 86.2°, and 86.3°, respectively), consistent with Co occupying the axial position of the trigonal bipyramidal Zr coordination sphere. Notably, a search of the Cambridge Structural Database (CSD) indicated that this sort of geometry about Zr, (3 L−Zr−L angles of 120° ± 2°) is unprecedented in the absence of a fifth donor ligand.

As shown in Figure 1 and Table 1, complexes **4**, **5**, and **6** have Zr−Co interatomic distances of 2.7315(5), 2.6280 (5), and 2.6309(5) Å, respectively. While large variations in reported covalent radii for Zr and Co exist in the literature,[12] the Zr−Co interatomic distances in **4**−**6** are shorter than the sum of the covalent radii of Zr and Co determined using most methods. More explicit evidence for a bond comes from comparison of the Zr−Co distances in **4**−**6** with those in the only two Zr−Co bonds that have been structurally determined to date, 2.705(1) and 2.617(1) Å in complexes $[SiMe_2N(4\text{-}CH_3C_6H_4)]_3Zr{-}Co(CO)_3L$ (L = CO and PPh_3, respectively), indicate that the Zr−Co distances in **4**−**6** are within the range of legitimate Zr−Co bonds.[13] It is worth noting that these previously characterized Zr−Co bonds, unlike those in **4**−**6**, are not supported or enforced by a ligand framework. In complexes **4**−**6**, it is possible that the close proximity of the Zr and Co atom is enforced by ligand geometry and is not the result of orbital overlap between Zr and Co; however, electrochemical consequences and DFT calculations, discussed later in this manuscript, suggest that Zr−Co interactions exist in **4**−**6** and are dative in nature, with the electron-rich, formally Co^{I} center donating electrons to the Lewis-acidic Zr^{IV} center. The shorter Co−Zr interatomic distances in **5** and **6** compared to **4** can be attributed to the more electron-rich ^{i}Pr phosphine substituents that impart more electron density on the cobalt center, strengthening its donation to Zr.

Assessment of the Redox Behavior of Heterobimetallic Co/Zr Complexes 4−6 Using Cyclic Voltammetry. As interatomic distances determined by X-ray crystallography suggest a Co→Zr interaction which is expected to decrease the electron density at Co in **4**, **5**, and **6**, the effect of this interaction on the redox properties of cobalt in these complexes was probed using cyclic voltammetry (CV). Interestingly, the CVs of **4**−**6** showed reductive events, although the nature of these reductions was different for each species (Figure 2B). These reductions are assigned as cobalt-based, since CVs of the zirconium complexes **1**−**3** did not contain any features within the tetrahydrofuran (THF) solvent window. Complex **4** showed a fully reversible reduction at −1.65 V. Although this appears to be a single reduction, even by differential pulse voltammetric (DPV) techniques, bulk electrolysis of a sample of **4** at −1.77 V required ∼2 electrons per molecule of **4** (1.94 e^-). Thus, the reversible reduction in the CV of **4** is assigned as a $2e^-$ process, as confirmed by bulk chemical reduction (vide infra).

The CV of complex **5** also possessed a reversible reduction at −1.64 V; however, in this case the reduction was followed by an immediate, irreversible reduction at −1.87 V. This can best be explained by an EEC mechanism, in which the first one-electron reduction is reversible, but

(12) Examples of discrepancies in covalent radii reported in the literature: (a) 1.75 Å + 1.26 Å = 3.01 Å (for l.s. Co) or 1.75 Å + 1.50 Å = 3.25 Å: Cordero, B.; Gómez, V.; Platero-Prats, A. E.; Revés, M.; Echeverría, J.; Cremades, E.; Barragán, F.; Alvarez, S. *Dalton Trans.* **2008**, 2832. (b) 1.54 Å + 1.11 Å = 2.65 Å: Pyykkö, P.; Atsumi, M. *Chem.—Eur. J.* **2009**, *15*, 186. (c) 1.45 Å + 1.16 Å = 2.61 Å: Pauling, L. *The Nature of the Chemical Bond*, 3rd ed.; Cornell University Press: Ithaca, NY, 1960. (d) 1.56 Å + 1.33 Å = 2.89 Å: Cambridge Structural Database, http://www.ccdc.cam.ac.uk/products/csd/radii/table.php4#symbol. (e) If the Co-Co (2.506 Å) and Zr-Zr (3.179 Å) distances in elemental cobalt and zirconium metal are divided by 2 to extract a typical covalent radius in a metal−metal bond, we obtain 1.59 Å + 1.25 Å = 2.84 Å: In *Table of Interatomic Distances and Configuration in Molecules and Ions*, Supplement 1956−1959, Special publication No. 18; Sutton, L. E., Ed.; Chemical Society: London, U.K., 1965.

(13) Jansen, G.; Schubart, M.; Findeis, B.; Gade, L. H.; Scowen, I. J.; McPartlin, M. *J. Am. Chem. Soc.* **1998**, *120*, 7239.

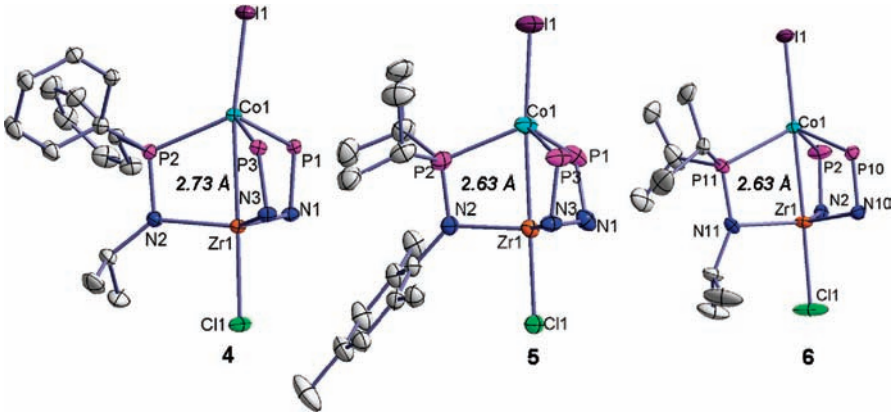

Figure 1. Displacement ellipsoid (50%) representations of **4**, **5**, and **6**. All hydrogen atoms and substituents on all but one phosphinoamide ligand have been omitted for clarity.

Table 1. Relevant Interatomic Distances (Å) and Angles (deg) in Complexes **4**–**6** and **8**

	4	5	6	8
Zr–Co	2.7315(5)	2.6280(5)	2.6309(5)	
Zr–N	2.107(2)	2.129(2)	2.109(3)	
	2.100(2)	2.131(2)	2.120(7)	
	2.101(2)	2.133(2)	2.096(8)	
Co–P	2.2933(7)	2.3645(10)	2.3418(8)	2.2109(5)
	2.3116(7)	2.3613(9)	2.334(10)	2.2109(5)
	2.2964(7)	2.3806(8)	2.369(10)	2.2109(5)
Zr–Cl	2.4226(7)	2.4450(7)	2.4508(10)	
Co–I	2.5434(4)	2.5837(4)	2.5497(4)	2.5455(3)
Cl–Zr–Co	178.94(2)	178.95(2)	177.70(5)	
I–Co–Zr	171.331(15)	174.86(2)	177.63(18)	
P–Co–P	109.46(3)	106.42(3)	107.4(2)	105.296(13)
	109.07(3)	111.78(3)	111.5(2)	105.296(13)
	104.89(3)	107.07(3)	108.4(5)	105.296(13)
N–Zr–N	117.82(8)	117.97(9)	118.6(3)	
	119.80(8)	121.5(9)	122.4(3)	
	118.31(8)	119.15(9)	117.72(12)	
N–Zr–Co	83.74(5)	86.38(7)	86.37(8)	
	83.45(6)	85.70(6)	86.0(3)	
	82.60(6)	86.51(6)	86.5(3)	

upon addition of a second electron, a chemical process occurs to generate a new species that cannot be reoxidized. Since electrochemical experiments were performed under an N_2 atmosphere, we propose that the features in the CV of **5** are attributed to rapid, irreversible N_2 binding upon reduction of **5** by $2e^-$ (this is further confirmed by bulk chemical reduction, vide infra).

Interestingly, we find that while the phosphine substituents on **4** and **5** should vary in electron-donating ability enough to affect the reduction potential of these Co centers, the reduction potentials for the first reduction of **4** and **5** are identical. It seems likely that this is a direct consequence of the stronger Zr–Co interaction in complex **5** based on the ~0.1 Å shorter Zr–Co interatomic distance. The CV of complex **6**, which has a Zr–Co distance identical to that of **5**, shows quasi-reversible reductions at −1.86 and −2.07 V. In this case, the reductions are presumably shifted to more negative potentials than those of **5** as a result of the more electron-releasing ^{i}Pr amide substituents.

To compare the reduction potentials of **4**–**6** with a similar compound lacking an electron-withdrawing Zr center, the CV of complex **8** was obtained.[8] As observed for the heterobimetallic complexes, the CV of **8** showed

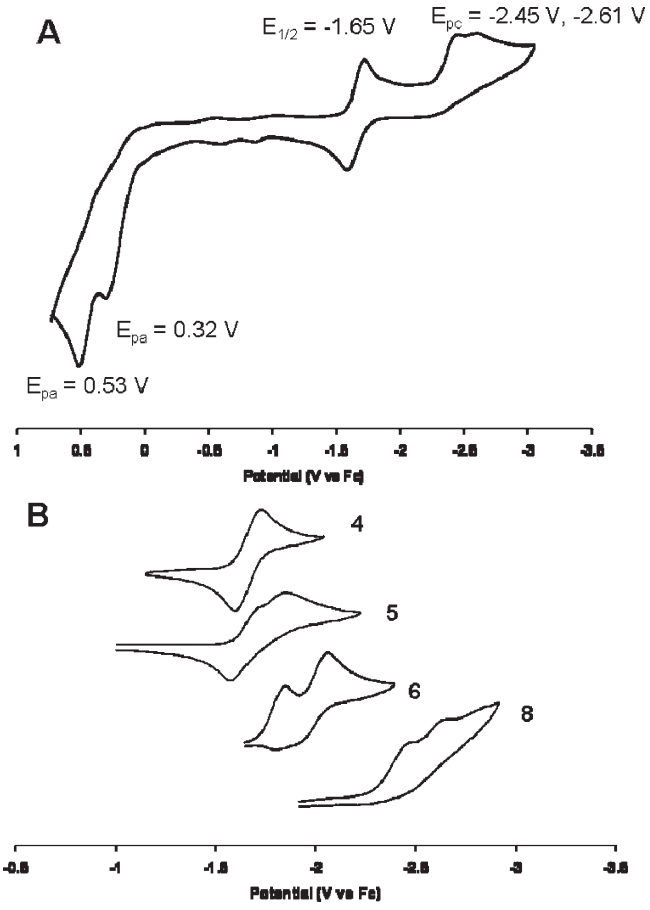

Figure 2. Full CV of complex **4** (A) and reductive portion of the CV of **4**, **5**, **6**, and **8** (B) (2 mM in 0.4 M [^{n}Bu$_4$N][PF$_6$] in THF; scan rate = 100 mV/s).

two irreversible reductive events (Figure 2B). However, these reductions occurred at −2.46 and −2.65 V, nearly 1 V more negative than the reduction potentials of the corresponding Co/Zr complex **4**. In light of this, it can be concluded that in complex **4** the electron-density on cobalt is significantly diminished with respect to **8**, thermodynamically favoring the reduced product, and raising the reduction potential. Thus, dative donation from Co to Zr has a dramatic effect on the redox activity of cobalt, allowing further reduction of the Co^I center at milder potentials.

Table 2. Oxidation and Reduction Potentials of Complexes **4**, **5**, **6**, and **8** as Determined Using Cyclic Voltammetry[a]

	4	5	6	8
Co^{III}/Co^{II}	0.53 V[d]	0.60 V[d]	0.25 V[d]	
Co^{II}/Co^{I}	0.32 V[d]	0.47 V[d]	−0.07 V[d]	0.57[d]
Co^{I}/Co^{0}	−1.65 V[b]	−1.64 V[b]	−1.86 V[c]	−2.49[c]
Co^{0}/Co^{-I}	−1.65 V[b]	−1.87 V[c]	−2.07 V[c]	−2.66[c]

[a] 2 mM analyte in 0.4 M [$^{n}Bu_4N$][PF_6] in THF; scan rate = 100 mV/s. [b] $E_{1/2}$ (reversible). [c] E_{pc} (irreversible or quasi-reversible). [d] E_{pa} (irreversible).

Scheme 3

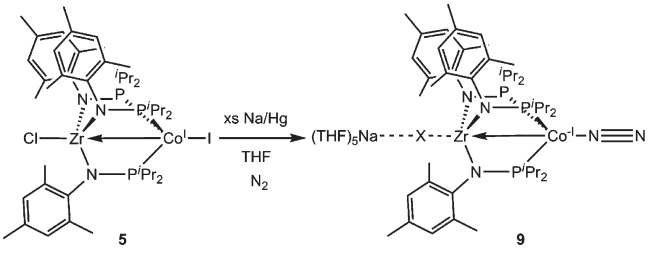

In addition, it is worth noting that the CVs of **4**−**6** in THF showed only irreversible Co^{II}/Co^{I} oxidation events, consistent with the inability to isolate Zr^{IV}/Co^{II} species prior to reduction (Table 2).[8] For example, the CV of **4** has only irreversible oxidative features at 0.32 and 0.53 V, implying that a Co^{II} species is unstable (Figure 2A).

Two-Electron Reduction of Heterobimetallic Co/Zr Complex 5 and Binding of Dinitrogen to the Reduced Species. As predicted by cyclic voltammetry, bulk samples of complexes **4**−**6** can be chemically reduced with excess Na/Hg in THF solution, resulting in a color change from green to red/brown. Notably, in all three complexes, addition of just 1 equiv of Na/Hg led to a 1:1 mixture of starting material and reduced product, indicating that reduction by two electrons is favored. As shown in Scheme 3, the product generated upon treatment of **5** with excess Na/Hg is diamagnetic and contains a dinitrogen moiety bound to cobalt, as indicated by IR spectroscopy ($\nu(N_2) = 2023\ cm^{-1}$).

The structure of this complex, [$N_2Co(^{i}Pr_2PN$-$Mes)_3ZrX$][$Na(THF)_5$] (**9**, where X = a mixture of Cl and I) was determined via X-ray crystallography and is shown in Figure 3. Upon reduction, the halide remaining on Zr exchanges with the NaI in solution, leading to significant crystallographic disorder between Cl^- and I^- which has been modeled adequately with occupancies of 73% I and 27% Cl in the structure of **9**. In addition to halide loss and dinitrogen binding, some noteworthy structural changes occur upon reduction of **5** to **9**. Most interestingly, the Zr−Co distance in **9** is 2.4112(3) Å, more than 0.2 Å shorter than the 2.6280(5) Å distance in **5**. This contraction of the intermetallic distance suggests that the increase in electron density upon reduction of Co leads to a stronger dative donation from Co to the Lewis acidic Zr center. The geometry about the Zr center continues to be trigonal bipyramidal, as was observed in the structure of **5**. While the Co center is still best described as tetrahedral, the P−Co−P angles are slightly expanded upon strengthening the Co−Zr interaction

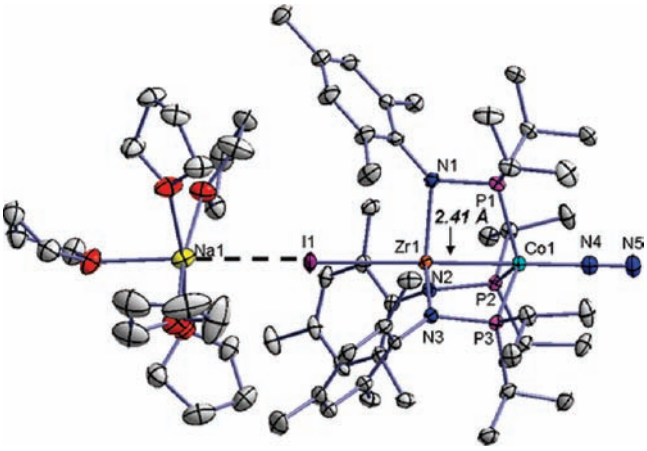

Figure 3. Diplacement ellipsoid (50%) representation of **9**. Hydrogen atoms have been omitted for clarity. Relevant bond distances (Å) and angles (deg): Zr1−Co1, 2.4112(3); Co1−N4, 1.8186(16); N4−N5, 1.120(2); Zr1−I1, 2.9722(7); Zr1−Cl1, 2.690(7); Na1−I1, 3.2695(12); Co1−P1, 2.1209(5); Co1−P2, 2.2153(5); Co1−P3, 2.2098(5); Zr1−N1, 2.1524; Zr1−N2, 2.1559(15); Zr1−N3, 2.1639(15); I1−Zr1−Co1, 178.560(17); N4−Co1−Zr1, 179.33(5); N1−Zr1−N2, 117.80(6); N2−Zr1−N3, 121.16(6); N1−Zr1−N3, 119.82(6); N1−Zr1−Co1, 96.35(4); N2−Zr1−Co1, 86.73(4); N3−Zr1−Co1, 85.93(4); P1−Co1−P2, 112.404(19); P2−Co1−P3, 113.80(2); P3−Co1−P1, 113.24(2).

(avg. P−Co−P angles are 108° and 113° in **5** and **9**, respectively), indicative of a distortion toward a trigonal bipyramid.

Both the relatively short N−N distance of 1.120(2) Å (in free N_2, N−N = 1.0975 Å) and the relatively high $\nu(N_2)$ (2023 cm^{-1} vs 2331 cm^{-1} in free N_2) suggest very little activation of the N_2 unit in complex **9** despite the seemingly low formal oxidation state (Co^{-I}).[14] Moreover, in comparing the N−N distance and $\nu(N_2)$ stretch for **9** with parameters for previously reported Co−N_2 complexes, it is found that the degree of N_2 activation in **9** is most consistent with Co^{I}−N_2 complexes, which have N−N distances ranging from 1.08 Å to 1.15 Å and $\nu(N_2)$ bands in the 2024−2125 cm^{-1} range.[15] In contrast, Co−N_2 complexes in the formal −1 or 0 oxidation state typically have lower $\nu(N_2)$ stretching frequencies (1830−1910 cm^{-1}) and longer N−N distances (1.15 Å to 1.19 Å).[15a,16] We attribute this to the involvement of the filled Co d orbitals in both σ and π-donation to Zr, disfavoring backbonding into the N−N antibonding orbitals of coordinated N_2, as supported by our DFT calculations (vide infra). Bourissou and co-workers note a similar shift to higher stretching frequency as a result of a dative Rh→B interaction

(14) Mackay, B. A.; Fryzuk, M. D. *Chem. Rev.* **2004**, *104*, 385.
(15) (a) Betley, T. A.; Peters, J. C. *J. Am. Chem. Soc.* **2003**, *125*, 10782. (b) Enemark, J. H.; Davis, B. R.; McGinnety, J. A.; Ibers, J. A. *Chem. Commun.* **1968**, 96. (c) Davis, B. R.; Payne, N. C.; Ibers, J. A. *Inorg. Chem.* **1969**, 2719. (d) Bianchini, C.; Peruzzini, M.; Zanobini, F. *Organometallics* **1991**, *10*, 3415. (e) Bianchini, C.; Mealli, C.; Meli, A.; Peruzzini, M.; Zanobini, F. *J. Am. Chem. Soc.* **1988**, *110*, 8725. (f) Egan, J. W.; Haggerty, B. S.; Rheingold, A. L.; Sendlinger, S. C.; Theopold, K. H. *J. Am. Chem. Soc.* **1990**, *112*, 2445. (g) Fout, A. R.; Basuli, F.; Fan, H.; Tomaszewski, J.; Huffman, J. C.; Baik, M.-H.; Mindiola, D. J. *Angew. Chem., Int. Ed.* **2006**, *45*, 3291.
(16) (a) Yamamoto, A.; Miura, Y.; Ito, T.; Chen, H. L.; Iri, K.; Ozawa, F.; Miki, K.; Sei, T.; Tanaka, N.; Kasai, N. *Organometallics* **1983**, *2*, 1429. (b) Hammer, R.; Klein, H.-F.; Schubert, U.; Frank, A.; Huttner, G. *Angew. Chem., Int. Ed. Engl.* **1976**, *15*, 612. (c) Cecconi, F.; Ghilardi, C. A.; Midollini, S.; Moneti, S.; Orlandini, A.; Bacci, M. *J. Chem. Soc., Chem. Commun.* **1985**, 731.

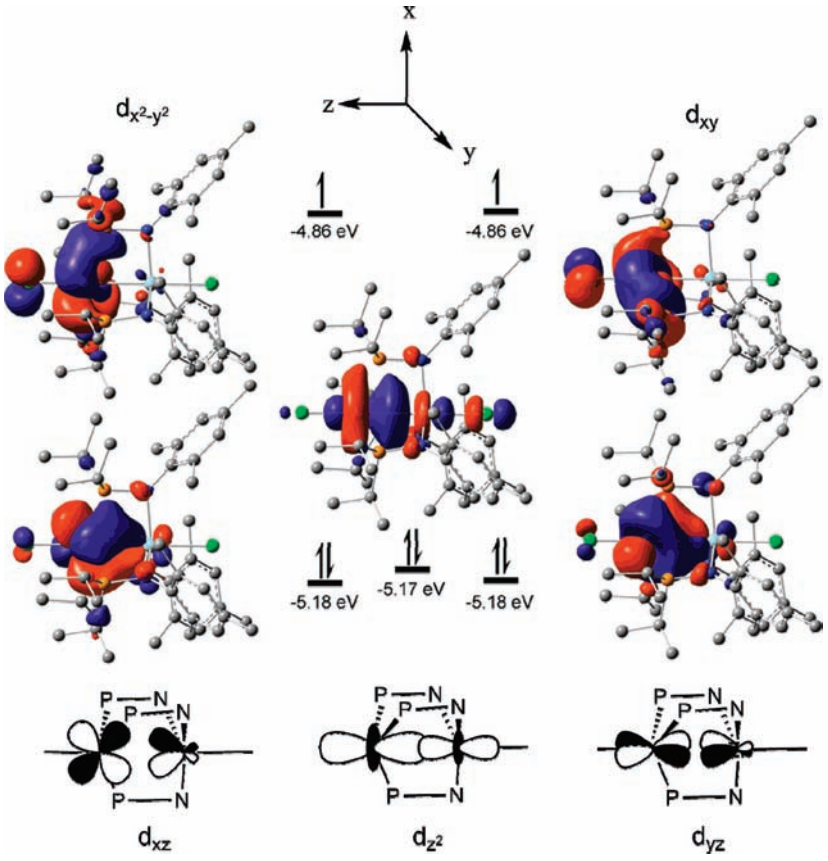

Figure 4. Calculated molecular orbital diagram of the frontier orbitals of **5** with orbital visualizations derived from natural orbital population analysis.

in their complex RhCl(CO)(diphosphine-borane).[2d] It is also noteworthy that the Zr−X distance (in both the case of Cl and I) is significantly elongated from that observed in typical Zr halide complexes. While this is due, at least in part, to the strong interaction with the Na^+ countercation, it is also likely that the electron rich Co center exerts a strong *trans* influence on Zr. Reduction of complexes **4** and **6** with Na/Hg also leads to diamagnetic red/brown products with dinitrogen bound to Co ($\nu(N_2)$ = 2019 and 1992 cm^{-1}, respectively), and the structures and characterization of these products will be reported in a future work.

Theoretical Investigation of Metal−Metal Interactions in Co/Zr Heterobimetallics using DFT. To better understand the interaction between the cobalt and zirconium atoms in this series of complexes, theoretical calculations were performed on an analogue of compound **5** and the reduced dinitrogen adduct, **9**. Geometry optimization and frequency calculations were carried out using the BP86 functional and a mixed basis set consisting of LANL2TZ(f) (Co,Zr), 6-311 + G(d) (Cl, N, P), and D95V (C, H) basis sets. Although the full molecules were used for our computational analyses starting from coordinates determined via X-ray crystallography, the I atom in **5** was replaced with Cl for simplicity.

The results of geometry optimization of **5** using DFT are in excellent agreement with experiment, as shown in Table 3. In accordance with our assignment of the cobalt atom as existing in the +1 oxidation state, the unpaired spin density resides almost exclusively on the cobalt atom (Supporting Information, Figure S14) and Mulliken population analysis predicts a spin density of 1.87 on the cobalt atom in **5**. Visualization of the frontier molecular orbitals of **5** reveals several interesting features relating to the interaction between the cobalt and zirconium atoms (Figure 4). Rather than the three-over-two d-orbital splitting pattern that would be predicted for a tetrahedral cobalt center, theory predicts a significant lowering of the energy of the Co d_{z^2} orbital in **5**. This stabilization appears to result from substantial orbital overlap between the Co and Zr d_{z^2} orbitals. Thus, donation of electron density from the filled Co d_{z^2} orbital to the empty Zr d_{z^2} orbital results in a net bonding interaction. In addition to this sigma bonding orbital, close inspection of the frontier orbitals also reveals two orbitals corresponding to the Co d_{xz} and d_{yz} orbitals that exhibit π-type bonding interactions with the Zr center. Furthermore, Mayer population analysis reveals a Co−Zr bond index of 0.73 as a result of these three interactions. Thus, electron density is clearly

Table 3. Selected Bond Lengths (Å) and Angles (deg) of **5** as Determined by Crystallography and Theoretical Calculations

	experimental (X-ray)	calculated (DFT)[a]
Zr−Co	2.6280(5)	2.666
Zr−Cl	2.4450(7)	2.440
Co−P1	2.3645(10)	2.378
Co−P2	2.3613(9)	2.384
Co−P3	2.3806(8)	2.380
Zr−N1	2.129(2)	2.136
Zr−N2	2.131(2)	2.147
Zr−N3	2.133(2)	2.132
Cl2−Zr−Co	178.95(2)	178.75

[a] Gaussian '03: BP86/LANL2TZ(f)/6-311 + G(d)/D95 V.

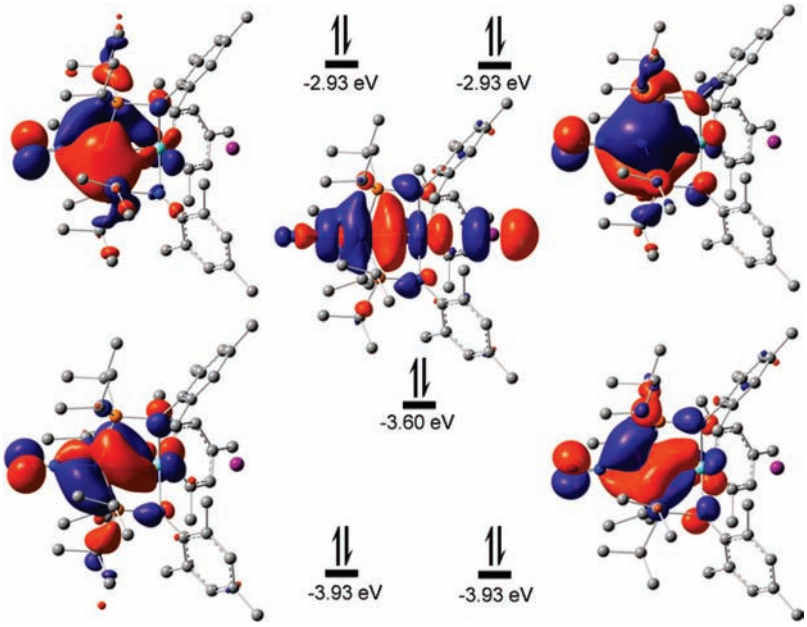

Figure 5. Calculated molecular orbital diagram of the frontier orbitals of **9** with visualizations of the corresponding molecular orbitals. The $Na(THF)_5^+$ unit has been omitted for clarity.

drawn away from the Co center by the Lewis acidic Zr atom, and it is to this dative-like interaction that we attribute the facile two-electron reduction of **5**.

In computational studies of **9**, it was necessary to include the THF-coordinated Na^+ countercation to obtain a geometry consistent with that determined using X-ray diffraction data. The calculated Co−Zr interatomic distance agrees well with the experimental value (2.41 Å vs. 2.42 Å, respectively), as does the N−N bond distance of the ligated dinitrogen moiety (1.12 Å vs. 1.14 Å, respectively). Moreover, the dinitrogen stretching frequency of 2025 cm^{-1} derived from the frequency calculation is nearly identical to the 2023 cm^{-1} frequency observed in the infrared spectrum of **9**.

The 0.23 Å reduction in the Co−Zr distance that accompanies the two-electron reduction of **5** to form **9** is intriguing, as it suggests that a stronger bonding interaction is forming between the two metal centers. Accordingly, the Co−Zr Mayer bond index is increased to 1.23 in **9**. As with complex **5**, visualization of the frontier orbitals reveals a discrete σ-bonding interaction between the two metal centers mediated by the Co and Zr d_{z^2} orbitals as well as two π-type bonding interactions originating from the d_{xz} and d_{yz} orbitals on Co (Figure 5). In addition to these interactions, examination of the highest occupied molecular orbitals (HOMOs), to which the two additional electrons have been added, reveals a noticeably greater bonding contribution between Co and Zr which was not present in **5**. We attribute the significantly higher Zr−Co bond order and shorter Zr−Co distance to this new bonding contribution.

With respect to the bonding interactions between Co and N_2, the elongation and diminished stretching frequency of the dinitrogen bond with respect to gaseous N_2 suggests activation of the N−N bond upon binding to the metal center, but to a far lesser extent than is typically seen in such low valent late transition metal dinitrogen complexes. The results of the theoretical investigation of **9** give some insight into the nature of this phenomenon. As evident in the molecular orbital surfaces in Figure 5, the molecular orbitals that house the Co−N_2 backbonding interactions are also involved in the π-type interactions between Co and Zr, and it appears that this diminishes the amount of electron density available for back-bonding into the N_2 π^* orbitals.

Conclusion

In summary, we have shown that tethering a Lewis acidic early transition metal such as Zr in close proximity to an electron-rich late transition metal leads to metal−metal interactions which are dative in nature. Evidence for Co→Zr interactions in **4**−**6** is provided by structural characterization data and computational studies using DFT. DFT calculations reveal that the interaction between Co and Zr occurs through both σ and π overlap of the metal d orbitals. Donation of electron density from Co to Zr has dramatic effects on the redox activity of Co, causing shifts of nearly 1 V to milder reduction potentials. The Zr center in these complexes plays the role of a Z-type metalloligand,[3] rendering these complexes analogous to recently reported "metallaboratranes" featuring M→B dative bonds. Much like transition metal boranes, the assignments of a formal oxidation to the metal centers in **4**−**6** and **9** is not informative. This is particularly evident in complex **9**, which would traditionally be assigned an oxidation state of Co^{-I} but has structural and spectroscopic features more consistent with a Co^{I} center. The polarized nature of dative metal−metal interactions such as those presented in this manuscript may prove advantageous in the activation of small molecule substrates. Furthermore, the ability of dative interactions in heterobimetallic complexes to facilitate multielectron redox activity at significantly milder potentials is a promising lead in the design of catalysts for redox transformations. Future studies will focus on the utility of these particular heterobimetallic complexes for small molecule activation reactions and also on new more flexible ligand systems to provide more opportunity for reversible metal−metal bond formation.

Experimental Section

General Considerations. All syntheses reported were carried out using standard glovebox and Schlenk techniques in the absence of water and dioxygen, unless otherwise noted. Benzene, pentane, diethyl ether, tetrahydrofuran, dichloromethane, and toluene were degassed and dried by sparging with N_2 gas followed by passage through an activated alumina column. Ethanol was dried over CaH_2 and distilled, followed by sparging with N_2 prior to use. All solvents were stored over 3 Å molecular sieves. Deuterated benzene and toluene were purchased from Cambridge Isotope Laboratories, Inc., degassed via repeated freeze−pump−thaw cycles, and dried over 3 Å molecular sieves. THF-d_8 was dried over Na/K alloy, vacuum-transferred, and degassed via repeated freeze−pump−thaw cycles. Solvents were frequently tested using a standard solution of sodium benzophenone ketyl in tetrahydrofuran to confirm the absence of oxygen and moisture. Ph_2PNH^iPr,[7] and complex **1**[5c] were synthesized using literature procedures. All other chemicals were purchased from Aldrich, Strem, or Alfa Aesar and used without further purification. NMR spectra were recorded at ambient temperature unless otherwise stated on a Varian Inova 400 MHz instrument. ^1H and ^{13}C NMR chemical shifts were referenced to residual solvent. ^{31}P NMR chemical shifts were referenced to 85% H_3PO_4. IR spectra were recorded on a Varian 640-IR spectrometer controlled by Resolutions Pro software. UV−vis spectra were recorded on a Cary 50 UV−vis spectrophotometer using Cary WinUV software. Elemental microanalyses were performed by Atlantic Microlab, Inc., Norcross, GA. Solution magnetic moments were measured using Evans' method.[17]

X-ray Crystallography Procedures. All operations were performed on a Bruker-Nonius Kappa Apex2 diffractometer, using graphite-monochromated Mo Kα radiation. All diffractometer manipulations, including data collection, integration, scaling, and absorption corrections were carried out using the Bruker Apex2 software.[18] Preliminary cell constants were obtained from three sets of 12 frames. Structures were solved using SIR-92,[19] and refined (full-matrix-least-squares) using the Oxford University Crystals for Windows program.[20] All ordered non-hydrogen atoms were refined using anisotropic displacement parameters; hydrogen atoms were fixed at calculated geometric positions and allowed to ride on the corresponding carbon atoms. Crystallographic parameters for all structures reported are summarized in Tables 4 and 5. Further crystallographic details may be found in the Supporting Information file and the accompanying CIF files.

Electrochemistry. Cyclic voltammetry measurements were carried out in a glovebox under a dinitrogen atmosphere in a one-compartment cell using a CH Instruments electrochemical analyzer. A glassy carbon electrode and platinum wire were used as the working and auxiliary electrodes, respectively. The reference electrode was $Ag/AgNO_3$ in THF. Solutions (THF) of electrolyte (0.40 M $[^nBu_4N][PF_6]$) and analyte (2 mM) were also prepared in the glovebox.

A standard H-type bulk electrolysis cell was used for bulk electrolysis measurements. The cathodic chamber was charged with crystalline complex **4** (20.6 mg, 0.0168 mmol) and both chambers were filled with 10 mL of a 0.1 M $[^nBuN_4][PF_6]$ solution in THF. Controlled potential electrolysis commenced at −1.77 V until the solution current was less than 0.5% of the initial value (3.14 C passed, in 62 min). This corresponds to 1.94 electron equivalents if you take into account the three toluene solvent molecules per complex in crystals of **4**.

Table 4. X-ray Diffraction Experimental Details for $ICo(Ph_2PN^iPr)_3ZrCl$ (**4**), $ICo(^iPr_2PNMes)_3ZrCl$ (**5**), and $ICo(^iPr_2PN^iPr)_3ZrCl$ (**6**)

	4	**5**	**6**
chemical formula	$C_{59}H_{67}ClCoIN_3P_3Zr$	$C_{45}H_{75}ClCoIN_3P_3Zr$	$C_{27}H_{63}ClCoIN_3P_3Zr$
fw	1223.63	1063.54	835.25
T (K)	120	120	120
λ (Å)	0.71073	0.71073	0.71073
a (Å)	10.8403(14)	27.8496(8)	15.1913(8)
b (Å)	14.4482(19)	53.0394(14)	18.1727(10)
c (Å)	18.620(2)	15.0536(4)	13.4668(7)
α (deg)	74.452(5)	90	90
β (deg)	82.637(5)	90	90
γ (deg)	86.324(6)	90	90
V (Å^3)	2785.1(6)	22236.1(10)	3717.7(3)
space group	*P*-1	*Fdd*2	*Pnma*
Z	2	16	4
D_{calc} (g/cm^3)	1.459	1.271	1.492
μ (cm^{-1})	12.13	12.05	17.78
R1, wR2[a] ($I > 2\sigma(I)$)	0.0299, 0.0778	0.0332, 0.0867	0.0300, 0.0620

[a] $R1 = \sum||F_o| - |F_c||/\sum|F_o|$, $wR2 = \{\sum w(F_o^2 - F_c^2)^2/\sum w(F_o^2)^2\}^{1/2}$.

Table 5. X-ray Diffraction Experimental Details for $(Ph_2PNH^iPr)_2CoI_2$ (**7**), $(Ph_2PNH^iPr)_3CoI$ (**8**), and $[N_2Co(^iPr_2PNMes)_3ZrX][Na(THF)_5]$ (**9**)

	7	**8**	**9**
chemical formula	$C_{30}H_{36}CoI_2N_2P_2$	$C_{45}H_{54}CoIN_3P_3$	$C_{65}H_{115}Cl_{0.27}CoI_{0.73}N_5NaO_5P_3Zr$
fw	799.32	915.70	1415.34
T (K)	120	120	120
λ (Å)	0.71073	0.71073	0.71073
a (Å)	20.6816(13)	14.8343(4)	14.7610(9)
b (Å)	17.3232(11)	14.8343(4)	24.6060(15)
c (Å)	19.5909(12)	74.260(2)	19.1884(11)
α (deg)	90	90	90
β (deg)	113.823(3)	90	90.284(3)
γ (deg)	90	120	90
V (Å^3)	6420.8(7)	14152.0(7)	6969.3(7)
space group	$P\,1\,2_1/c\,1$	*R*-3*c*	$P\,1\,2_1/n\,1$
Z	8	12	4
D_{calc} (g/cm^3)	1.654	1.289	1.349
μ (cm^{-1})	25.79	11.51	8.47
R1, wR2[a] ($I > 2\sigma(I)$)	0.0207, 0.0469	0.0227, 0.0542	0.0330, 0.0721

[a] $R1 = \sum||F_o| - |F_c||/\sum|F_o|$, $wR2 = \{\sum w(F_o^2 - F_c^2)^2/\sum w(F_o^2)^2\}^{1/2}$.

Computational Details. All calculations were performed using Gaussian03-E.01[21] for the Linux operating system. DFT calculations were carried out using a combination of Becke's 1988 gradient-corrected exchange functional[22] and Perdew's 1986 electron correlation functional[23] (BP86). For open shell systems, unrestricted wave functions were used in energy calculations. A mixed-basis set was employed, using the LANL2TZ(f) triple-ζ basis set with effective core potentials for cobalt and zirconium,[24−27] Gaussian03's internal 6-311+G(d) for atoms bonded directly to the metal centers (nitrogen, phosphorus,

(17) (a) Sur, S. K. *J. Magn. Reson.* **1989**, *82*, 169. (b) Evans, D. F. *J. Chem. Soc.* **1959**, 2003.
(18) *Apex2, Version 2 User Manual, M86-E01078*; Bruker Analytical X-ray Systems: Madison, WI, 2006.
(19) Altomare, A.; Cascarano, G.; Giacovazzo, G.; Guagliardi, A.; Burla, M. C.; Polidori, G.; Camalli, M. *J. Appl. Crystallogr.* **1994**, *27*, 435.
(20) Betteridge, P. W.; Carruthers, J. R.; Cooper, R. I.; Prout, K.; Watkin, D. J. *J. Appl. Crystallogr.* **2003**, *36*, 1487.
(21) Frisch, M. J. et al. Gaussian, Inc.: Wallingford, CT, 2004.
(22) Becke, A. D. *Phys. Rev. A* **1988**, *38*, 3098.
(23) Perdew, J. P. *Phys. Rev. B* **1986**, *33*, 8822.
(24) Hay, P. J.; Wadt, W. R. *J. Chem. Phys.* **1985**, *82*, 299–310.
(25) Roy, L. E.; Hay, P. J.; Martin, R. L. *J. Chem. Theory Comput.* **2008**, *4*, 1029–1031.
(26) Ehlers, A. W.; Böhme, M.; Dapprich, S.; Gobbi, A.; Höllwarth, A.; Jonas, V.; Köhler, K. F.; Stegmann, R.; Veldkamp, A.; Frenking, G. *Chem. Phys. Lett.* **1993**, *208*, 111–114.
(27) Hay, P. J.; Wadt, W. R. *J. Chem. Phys.* **1985**, *82*, 270–283.

and chlorine), and Gaussian03's internal LANL2DZ basis set (equivalent to D95 V[28]) for carbon and hydrogen. Using crystallographically determined geometries as a starting point, when available, the geometries were optimized to a minimum, followed by analytical frequency calculations to confirm that no imaginary frequencies were present. Mayer bond order analysis[29] was performed with the routines included in the Gaussian03 package.

MesNHP^{i}Pr$_2$. A solution of 2,4,6-trimethylaniline (5.00 g, 37.0 mmol) in Et_2O (100 mL) was cooled to 0 °C in an ice bath. To this was added ^{n}BuLi (25.0 mL, 1.6 M in hexanes, 40.7 mmol) dropwise over 20 min. The resulting solution was allowed to warm slowly to room temperature, resulting in the formation of a white precipitate, then refluxed for 30 min to ensure complete reaction. The resulting suspension was added dropwise to a stirring solution of ^{i}Pr$_2$PCl (5.88 mL, 37.0 mmol) in Et_2O (100 mL) at −78 °C. Upon warming slowly to room temperature, the mixture became slightly yellow with a white LiCl precipitate. After stirring for 1 h, the reaction mixture was filtered through a pad of Celite, and solvent was removed from the filtrate in vacuo. The resulting oily residue was redissolved in Et_2O and filtered through a plug of silica gel. Removal of the solvent in vacuo yielded analytically pure product as a yellow oil (7.64 g, 82.2%). ^{1}H NMR (400 MHz, C_6D_6): δ = 6.79 (s, 2H, Mes), 3.16 (d, 1H, $^2J_{H-P}$ = 9.2 Hz, NH), 2.38 (s, 6H, Mes), 2.21 (s, 3H, Mes), 1.57 (m, 2H, C*H*(CH$_3$)$_2$), 1.04 (m, 12H, CH(C*H*$_3$)$_2$). ^{31}P{^{1}H} NMR (161.8 MHz, C_6D_6): δ = 57.7 (br, s). ^{13}C NMR (100.5 MHz, C_6D_6): δ = 142.0 ($^2J_{C-P}$ = 9.9 Hz), 130.4, 129, 127.8, 28.3 ($^1J_{C-P}$ = 16.8 Hz), 20.4, 19.0, 18.8, 17.3. Anal. Calcd for $C_{15}H_{26}NP$: C, 71.68; H, 10.43; N, 5.57. Found: C, 71.75; H, 10.66; N, 5.55.

^{i}Pr$_2$PNH^{i}Pr. A solution of isopropylamine (4.29 g, 72.5 mmol) in benzene (100 mL) was cooled to 0 °C. To this was added ^{i}Pr$_2$PCl (4.25 mL, 29.0 mmol) dropwise while stirring. The resulting solution was allowed to warm to room temperature over 1 h to ensure completion of the reaction. Upon warming to room temperature the solution became viscous. After completion, the viscous solution was filtered through a plug of silica gel. Removal of the solvent in vacuo yielded analytically pure product as a clear colorless liquid (4.43 g, 87.2%). ^{1}H NMR (400 MHz, C_6D_6): δ 2.99 (m, N-^{i}Pr, 1H), 1.33 (m, P-^{i}Pr, 2H), 0.95 (d, N-^{i}Pr, 3H), 0.92 (m, P-^{i}Pr, 6H), 0.56 (s, NH, 1H). ^{31}P{^{1}H} NMR (161.8 MHz, C_6D_6): δ 57.6 (br, s). ^{13}C NMR (100.5 MHz, C_6D_6): δ 49.0 ($^2J_{C-P}$ = 34 Hz), 26.4 ($^1J_{C-P}$ = 15.1), 26.2 ($^2J_{C-P}$ = 7.1), 19.4 ($^3J_{C-P}$ = 25.18), 17.2 ($^2J_{C-P}$ = 10.07). Owing to the increased oxygen sensitivity of this ligand, repeated elemental analysis samples analyzed as the oxidized form (^{i}Pr$_2$P(=O)NH^{i}Pr). Anal. Calcd for $C_9H_{22}NPO$: C, 56.52; H, 11.59; N, 7.32. Found: C, 56.29; H, 11.76; N, 7.15.

(^{i}Pr$_2$PNMes)$_3$ZrCl (2). A solution of MesNHP^{i}Pr$_2$ (1.046 g, 4.162 mmol) in Et_2O (50 mL) was cooled to −78 °C. To this was added ^{n}BuLi (2.6 mL, 1.6 M in hexanes, 4.2 mmol) dropwise over 10 min. The resulting yellow/orange solution was warmed to room temperature and stirred for 2 h. The solution was then cooled again to −78 °C, and $ZrCl_4$ (0.323 g, 1.39 mmol) was added portionwise as a solid. The reaction mixture was warmed to room temperature and stirred for 12 h. Volatiles were removed from the solution in vacuo, and the resulting solids were extracted with CH_2Cl_2 (30 mL) and filtered through a pad of Celite to remove LiCl. The volume of the filtrate was reduced to 10 mL in vacuo. The resulting supersaturated solution was layered with pentane and cooled to −35 °C to yield analytically pure colorless crystals of **2** (0.772 g, 63.4%). ^{1}H NMR (400 MHz, C_6D_6): δ = 6.84 (s, 6H, Mes), 2.48 (s, 18H, Mes), 2.34 (m, 6H, C*H*(CH$_3$)$_2$), 2.19 (s, 9H, Mes), 1.30 (m, 18H, CH(C*H*$_3$)$_2$), 1.16 (m, 18H, CH(C*H*$_3$)$_2$). ^{31}P{^{1}H} NMR (161.8 MHz, C_6D_6): δ = 9.49 (s). ^{13}C NMR (100.5 MHz, C_6D_6): δ = 148.7, 133.3, 131.9, 129.3, 34.5, 21.9, 21.7, 20.8. Anal. Calcd for $C_{45}H_{75}ClN_3P_3Zr$: C, 61.58; H, 8.61; N, 4.79. Found: C, 61.09; H, 8.47; N, 4.61.

(^{i}Pr$_2$PN^{i}Pr)$_3$ZrCl (3). A solution of ^{i}Pr$_2$PNH^{i}Pr (2.589 g, 10.06 mmol) in Et_2O (100 mL) was cooled to −78 °C. To this was added ^{n}BuLi (6.33 mL, 1.6 M in hexanes, 10.1 mmol) dropwise over 10 min. The resulting yellow/orange solution was warmed to room temperature and stirred for 3 h. The solution was then cooled back to −78 °C, and $ZrCl_4$ (0.800 g, 3.43 mmol) was added portionwise as a solid. This reaction mixture was then warmed to room temperature and stirred for 12 h. Volatiles were removed from the solution in vacuo, and the resulting solids were extracted with CH_2Cl_2 (20 mL) and filtered through a pad of Celite to remove LiCl. The volume of the filtrate was reduced to 5 mL in vacuo. The resulting supersaturated solution was layered with pentane and cooled to −35 °C for 12 h. The mother liquor was decanted to yield analytically pure colorless crystals of **3**. The decanted mother liquor was removed in vacuo, and the resulting solid was repeatedly washed with pentane to precipitate a pure colorless solid (0.727 g, 32.7%). ^{1}H NMR (400 MHz, C_6D_6): δ = 3.95 (m, 3H, NCH), 2.06 (m, 6H, PCH), 1.60 (d, 18H, NC(C*H*$_3$)$_2$), 1.17 (m, 36H, PC(C*H*$_3$)$_2$). ^{31}P{^{1}H} NMR (161.8 MHz, C_6D_6): δ = 1.5 (br, s). ^{13}C NMR (100.5 MHz, C_6D_6): δ = 52.7, 29.0, 26.9, 21.6, 19.1.Owing to the increased oxygen sensitivity of this complex, repeated elemental analysis samples analyzed as the mono-oxidized compound (^{i}Pr$_2$P(=O)N^{i}Pr)(^{i}Pr$_2$PN^{i}Pr)$_2$ZrCl. Anal. Calcd for $C_{27}H_{63}ClN_3P_3ZrO$: C, 48.74; H, 9.54; N, 6.31. Found: C, 48.41; H, 9.69; N, 6.15.

ICo(Ph$_2$PN^{i}Pr)$_3$ZrCl (4). Solid **1** (1.502 g, 1.76 mmol) and solid CoI_2 (0.551 g, 1.76 mmol) were combined in THF (15 mL) and stirred for 4 h at room temperature. The resulting dark green reaction solution was filtered through Celite, and solvent was removed from the volatiles in vacuo. The remaining green solids were extracted with toluene (10 mL) and filtered through Celite. The filtrate was cooled to −35 °C overnight to yield **4** as dark green crystalline solids. (1.137 g, 62.2%). Crystals for X-ray diffraction were grown by cooling a toluene/pentane solution to −35 °C. ^{1}H NMR (400 MHz, C_6D_6): δ = 14.22 (br s, Ph), 3.45 (br, (C*H*(CH$_3$)$_2$), 1.66 (br s, (CH(C*H*$_3$)$_2$), −5.57 (br, Ph), −7.01 (br s, Ph). UV−vis (C_6H_6) λ_{max}, nm (ε): 588 (190), 689 (140), 709 (130), 800 (240), 872 (610). Evans' method (C_6D_6): 2.92 μ_B. Anal. Calcd for $C_{45}H_{51}ClCoIN_3P_3Zr$: C, 52.00; H, 4.95; N, 4.04. Found: C, 51.17; H, 4.99; N, 3.94.

ICo(^{i}Pr$_2$PNMes)$_3$ZrCl (5). Solid **2** (1.641 g, 1.87 mmol) and solid CoI_2 (0.585 g, 1.87 mmol) were combined in CH_2Cl_2 and stirred for 48 h at room temperature. The resulting bright green solution was filtered through Celite, and solvent was removed from the filtrate in vacuo. The remaining green solids were washed with copious amounts of pentane and dried in vacuo to yield analytically pure **5** as a bright green solid (1.571 g, 79.0%). Crystals suitable for X-ray diffraction were grown via slow evaporation of a concentrated CH_2Cl_2 solution. ^{1}H NMR (400 MHz, C_6D_6): δ = 12.98 (br s, iPr-Me), 7.01 (s, Mes-Me), 2.54 (br s, iPr-Me), 1.95 (s, Mes-Me), −1.92 (br, Mes-Ar). UV−vis (C_6H_6) λ_{max}, nm (ε): 654 (190), 894 (350). Evans' method (C_6D_6): 2.87 μ_B. Anal. Calcd for $C_{45}H_{75}ClCoIN_3P_3Zr$: C, 50.82; H, 7.11; N, 3.95. Found: C, 49.69; H, 7.09; N, 3.79.

ICo(^{i}Pr$_2$PN^{i}Pr)$_3$ZrCl (6). Solid **3** (0.637 g, 9.81 mmol) and solid CoI_2 (0.307 g, 9.81 mmol) were combined in CH_2Cl_2 and stirred for 15 h at room temperature. The resulting green solution was filtered through Celite, and the solvent was removed from the filtrate in vacuo. The remaining green solids were repeatedly washed with diethyl ether and dried in vacuo to yield analytically pure product as a green solid (0.382 g, 46.5%). Crystals suitable for X-ray diffraction were grown via slow diffusion of pentane into a concentrated toluene solution. ^{1}H NMR (400 MHz, C_6D_6): δ = 70.6 (s br, P-CH), 8.05 (s br, P-iPrMe), 3.26 (s br, N−CH), 1.92 (s br, N-iPrMe), −1.68

(28) Dunning, T. H.; Hay, P. J. In *Modern Theoretical Chemistry*; Schaefer, H. F., Ed.; Plenum: New York, 1976; Vol. 3, p 1−28.
(29) Mayer, I. *Int. J. Quantum Chem.* **1986**, *29*, 477–483.

(s br, P-iPrMe). UV−vis (C_6H_6) λ_{max}, nm (ε): 691.0 (180), 724.9 (210), 744.0 (230), 767.9 (290), 873.9 (240). Evans' method (C_6D_6): 3.10 μ_B. Anal. Calcd for $C_{27}H_{63}ClCoIN_3P_3Zr$: C, 38.83; H, 7.60; N, 5.03. Found: C, 38.77; H, 7.62; N, 5.00.

($Ph_2PNH^iPr)_2CoI_2$ (7). Solid CoI_2 (0.176 g, 0.562 mmol) and Ph_2PNH^iPr (0.410 g, 1.69 mmol) were combined in THF (15 mL), and the resulting brick red solution was stirred for 4 h at room temperature. Solvent was removed from this solution in vacuo, and the resulting red solids were extracted into benzene (5 mL) and filtered through Celite. The brick red filtrate was then layered with pentane (15 mL) and allowed to sit for 12 h at room temperature to obtain **7** as a pure red crystalline product (0.182 g, 40.4%). Crystals of **7** suitable for X-ray diffraction were grown via vapor diffusion of pentane into a concentrated benzene solution of **7**. ^{1}H NMR (400 MHz, C_6D_6): δ = 15.94 (br s, Ph), 4.66 (br s, Ph), 4.86 (br s, CH(CH_3)$_2$), −10.0 (br, CH(CH_3)$_2$), −10.8 (br s, Ph). UV−vis (C_6H_6) λ_{max}, nm (ε): 486 (1600), 677 (1040), 715 (1390), 782 (1100). Evans' method (C_6D_6): 4.38 μ_B. Anal. Calcd for $C_{30}H_{36}CoI_2N_2P_2$: C, 45.08; H, 4.54; N, 3.50. Found: C, 45.34; H, 4.46; N, 3.48.

($Ph_2PNH^iPr)_3CoI$ (8). Solid CoI_2 (0.582 g, 1.86 mmol) and Ph_2PNH^iPr (1.583 g, 6.51 mmol) were combined in THF (15 mL) at room temperature, initially generating a brick red solution of **7**. To this vigorously stirred mixture was added Zn powder (0.608 g, 9.30 mmol). After 4 h of vigorous stirring, the resulting green solution was filtered away from the excess Zn. The solvent was removed from the filtrate in vacuo, and the resulting green residue was extracted into toluene (10 mL) and filtered to remove Zn salts. The green toluene solution was concentrated to 5 mL and layered with pentane (15 mL). After storage for 12 h at −35 °C, **8** was isolated as green crystals (1.129 g, 66.4%). Note: Over time in solution, **8** disproportionates to form **7** even at low temperature. Thus, the yield reported above corresponds to material that is only ∼85−90% pure, with red/brown powder of **7** present. Spectroscopic and elemental analysis data was collected on crystals of **8** that were mechanically separated from this mixture. Crystals suitable for X-ray diffraction were grown via layering a concentrated benzene solution with pentane. ^{1}H NMR (400 MHz, C_6D_6): δ = 79.5 (br, Ph), 11.17 (br s, Ph), 7.03 (br s, CH(CH_3)$_2$) 2.96 (br s, CH(CH_3)$_2$), 0.64 (br s, Ph). UV−vis (C_6H_6) λ_{max}, nm (ε): 611 (130), 683 (150), 955 (280). Evans' method (C_6D_6): 2.89 μ_B. Anal. Calcd for $C_{45}H_{54}CoIN_3P_3$: C, 59.02; H, 5.94; N, 4.59. Found: C, 58.94; H, 5.94; N, 4.58.

[$N_2Co(^iPr_2PNMes)_3ZrX$][$Na(THF)_5$] (9). A 0.5% Na/Hg amalgam was prepared from 0.0057 g Na (0.25 mmol) and 1.1 g Hg. To this vigorously stirred amalgam in 10 mL of THF was added a solution of **5** (0.1056 g, 0.0993 mmol) in THF (5 mL). The solution immediately began to change color from green to red. After 2 h, the resulting red solution was filtered away from the amalgam, and the solvent was removed from the filtrate in vacuo. Solvent was extracted back into THF and filtered through Celite. Layering the resulting concentrated red solution with pentane and cooling to −35 °C resulted in red crystals of **9** (0.0879 g, 61.5%). Crystals suitable for X-ray diffraction were grown via vapor diffusion of pentane into a concentrated THF solution of **9** at −35 °C. ^{1}H NMR (400 MHz, C_6D_6): δ = 6.77 (s, 6H, Mes), 3.36 (br m, 20H, THF), 3.03 (m, 6H, CH(CH_3)$_2$), 2.51 (s, 18H, Mes-Me), 2.13 (s, 9H, Mes-Me), 1.79 (m, 18H, CH(CH_3)$_2$), 1.57 (m, 18H, CH(CH_3)$_2$), 1.24 (br m, 20H, THF). ^{31}P{^{1}H} NMR (162 MHz, C_6D_6): δ = 43 ppm (br s). IR (KBr solution cell, THF): 2024 cm^{-1}. UV−vis (C_6H_6) λ_{max}, nm (ε): 509 (410), 676 (sh). The lability of the dinitrogen ligand and the overall instability of **9** precluded the collection of satisfactory combustion analysis data. Repeated samples consistently analyzed low for %N, as well as %C.

Acknowledgment. This work was supported by the gracious startup funds of Brandeis University. The authors are grateful to Nate Szymczak and Jonas C. Peters for their assistance with bulk electrolysis experiments. We thank D. Kellenberger and R. Rotstein for their assistance with X-ray crystallography.

Supporting Information Available: Experimental details, variable temperature ^{1}H NMR data for **2** and **3**, complete cyclic voltammetry data for **4**−**6** and bulk electrolysis data for **4**, crystallographic data for **4**−**9** (in CIF format) and additional computational detials. This material is available free of charge via the Internet at http://pubs.acs.org.